Supporting Information

Reaction between Ag_{17}^+ and acetylene outside the mass spectrometer: Dehydrogenation in the gas phase

Madhuri Jash, Rabin Rajan J. Methikkalam, Mohammad Bodiuzzaman, Ganesan Paramasivam, and Thalappil Pradeep*

DST Unit of Nanoscience (DST UNS) and Thematic Unit of Excellence (TUE), Department of Chemistry, Indian Institute of Technology Madras, Chennai 600 036, India

*To whom correspondence should be addressed. E-mail: pradeep@iitm.ac.in

Table of Contents

EXPERIMENTAL SECTION

Reagents and Materials

Silver nitrate ($AgNO_3$) was purchased from Rankem India, sodium borohydride ($NaBH_4$, 98%), sodium borodeuteride ($NaBD_4$, 98 atom% D) and triphenylphosphine (TPP) were purchased from Sigma-Aldrich. HPLC grade methanol (MeOH) was from Finar chemicals and analytical grade chloroform ($CHCl_3$) was from Rankem India. All the chemicals were used without further purification. Millipore water, with a resistivity of 18.2 MΩ.cm was used for the synthesis purpose.

Synthesis

The cluster $[Ag_{18}H_{16}(TPP)_{10}]^{2+}$ was synthesized by following our previous method, a modified method of a reported one. About 20 mg of $AgNO_3$ was dissolved in 5 mL of MeOH followed by the addition of 70 mg of triphenylphosphine in 10 mL of chloroform, under stirring at room temperature. After 20 minutes of reaction, 6 mg of $NaBH_4$ in 0.5 mL of ice cold water was added dropwise to the reaction mixture, which changed the color immediately from colorless to light yellow. Then the reaction was continued for three hours in dark condition to avoid any further oxidation of silver. The light yellow reaction mixture became dark green after three hours of continuous stirring, which indicated the formation of $[Ag_{18}H_{16}(TPP)_{10}]^{2+}$ cluster. The mixture of solvents was then vacuum evaporated and the excess silver precursor and $NaBH_4$ were removed by washing with 20-22 mL of cold Millipore water. Then the solid material consisting of $[Ag_{18}H_{16}(TPP)_{10}]^{2+}$ cluster was extracted with 2 mL of methanol and centrifuged for 5 minutes at 5,000 rpm to remove the excess TPP ligand. The deep green $[Ag_{18}H_{16}(TPP)_{10}]^{2+}$ cluster solution was used for further characterizations like UV-Vis and ESI MS. For all of our mass spectrometric experiments in LTQ, the above mentioned green cluster solution was diluted to 10 times by using methanol. For synthesizing the $[Ag_{18}D_{16}(TPP)_{10}]^{2+}$, in the synthesis procedure, $NaBH_4$ was replaced by $NaBD_4$.

Instrumentation

The optical absorption spectra of clusters were measured using a Perkin Elmer Lambda 25 UV-Vis spectrometer in the range of 200-1100 nm with a band pass filter of 1 nm. Waters Synapt G2Si HDMS instrument (abbreviated as G2Si subsequently) with electrospray ionization (ESI) source was used to record the high resolution mass spectra (HRMS) of $[Ag_{18}H_{16}(TPP)_{10}]^{2+}$ and $[Ag_{18}D_{16}(TPP)_{10}]^{2+}$ in positive ion mode. This mass spectrometer is equipped with electrospray source, quadrupole ion guide/trap, ion mobility cell and time of flight analyzer. For HRESI MS of the clusters, an optimized condition including a flow rate of 30 µL/min, a capillary voltage of 2 kV, a cone voltage and source offset of 0 V was used. All other experiments, related to the naked clusters and their reactions with acetylene described in this paper were carried out by using Thermo Scientific LTQ XL Linear Ion Trap Mass Spectrometer (abbreviated as LTQ subsequently) with a home-built nano-ESI source. The instrumental set-up of LTQ with nano-ESI source was described in details in our previous publication. To obtain a well-resolved MS signal the optimized conditions were, flow rate: 3 µL/min; ionization spray voltage: 3 kV; capillary temperature: 250 °C; capillary voltage (abbreviated as CV): 45 V and tube lens voltage (abbreviated as TV): 100 V. All the mass spectrometric measurements were done in the positive ion mode and 25 psi N_2 was used as the nebulizing gas. In this LTQ, CID was done by selecting a ion with a specific mass to charge ratio (m/z) by changing the radiofrequency (RF) and direct current, then colliding the ion with helium (He) gas inside the trap. Mass analysis of CID was done based on the ejected ions out of the trap. Multiple stages tandem mass spectrometry was also

performed in this instrument where a product ion, formed by CID experiment, was again selected for the next level CID experiment. These types of tandem mass spectrometry are also called MS^n experiment, where n = number of product ion stages. During all the CID experiments, the following parameters were kept constant; injection time 300 ms, microscans 5, activation time 30 ms, activation Q value 0.25.

COPUTATIONAL DETAILS

The ion/molecule reaction between acetylene and Ag_{17}^+ leads to dehydrogenation of acetylene and formation of hydrogen molecule/s and adducts such as $[Ag_{17}(C{\equiv}CH)_2]^+$, $[Ag_{17}(C{\equiv}CH)_4]^+$ and $[Ag_{17}(C{\equiv}CH)_6]^+$. All the structures were optimized using density functional theory (DFT) using the Gaussian 09 software.[1] Vibrational frequencies were calculated for all the optimized monocationic structures to ensure that it corresponds to a lower minimum. For the optimized structures of Ag_{17}^+, $[Ag_{17}(C{\equiv}CH)_2]^+$, $[Ag_{17}(C{\equiv}CH)_4]^+$ and $[Ag_{17}(C{\equiv}CH)_6]^+$, HOMO-LUMO gaps were calculated. During the optimization of adduct structure $[Ag_{17}(C{\equiv}CH)_2]^+$, other possible forms of acetylene adducts such as $[Ag_{17}(HC{\equiv}CH)]^+$, $[Ag_{17}(HC{\equiv}CH)_2]^+$, $[Ag_{17}(C_4H_2)]^+$ and $[Ag_{17}(C{\equiv}CH)]^+$ have also been optimized along with their binding energy values to know their possibility of formation. The mechanism of formation of hydrogen molecule/s was studied computationally when even number of acetylene molecules react with Ag_{17}^+. Whereas, for odd number of acetylene interaction, the intermediate does not end up with energetically favourable product or hydrogen molecule formation. We have also optimised the structures of $[Ag_{17}(C{\equiv}CH)]^+$ and [C≡CH], generated during the CID experiments of $[Ag_{17}(C{\equiv}CH)_2]^+$. The geometric optimization of the $[Ag_{17}(C{\equiv}CH)_2]^+$ cluster was done using restricted (closed electron shell) DFT in g09. The restricted occupancy of electrons allows 2 electrons for one MO. The calculated HOMO-LUMO gap of the cationic cluster is found to be 0.79 eV. The geometric optimization of $[Ag_{17}(C{\equiv}CH)]^+$ fragment was done using unrestricted (open shell) DFT in g09 by keeping its spin multiplicity as 2. The unrestricted occupancy of electrons splits the MOs into alpha and beta MOs either with a single free spin-up or spin-down electron respectively. The calculated HOMO-LUMO gap of the cationic cluster is 0.21 eV. The [C≡CH] fragment exists in its neutral form having an odd electron system with spin multiplicity 2. The calculated HOMO-LUMO gap is 1.11 eV. The 1s electron of H atom contributes to the beta π-bonding orbital of beta MOs of C_2H through sp^2 hybridization and the LUMO is made up of σ* anti-bonding orbital of beta MOs.
The binding energies were calculated using the following equation,

$$\text{binding energy} = E_{complex} - [E_{monomer1} + E_{monomer2}]$$

where $E_{complex}$ is the energy of $[Ag_{17}(C{\equiv}CH)_n]^+$, $E_{monomer1}$ is the energy of Ag_{17}^+, and $E_{monomer2}$ is the energy of n number of (C≡CH), where n = 1, 2, 4 and 6. In other cases (without dehydrogenation of acetylene), $E_{complex}$ is the energy of $[Ag_{17}(HC{\equiv}CH)_n]^+$, $E_{monomer1}$ is the energy of Ag_{17}^+, and $E_{monomer2}$ is the energy of n number of (HC≡CH), where n = 1 and 2.

[1] M. J. Frisch, G. W. Trucks, H. B. Schlegel, G. E. Scuseria, M. A. Robb, J. R. Cheeseman, G. Scalmani, V. Barone, B. Mennucci, G. A. Petersson, H. Nakatsuji, M. Caricato, X. Li, H. P. Hratchian, A. F. Izmaylov, J. Bloino, G. Zheng, J. L. Sonnenberg, M. Hada, M. Ehara, et al. *Gaussian 09*, Revision B.01. Gaussian 09, Revision B.01; Gaussian, Inc.: Wallingford, CT, 2009.

Supporting information 1

Characterisation of $[Ag_{18}H_{16}(TPP)_{10}]^{2+}$ and $[Ag_{18}D_{16}(TPP)_{10}]^{2+}$ clusters:

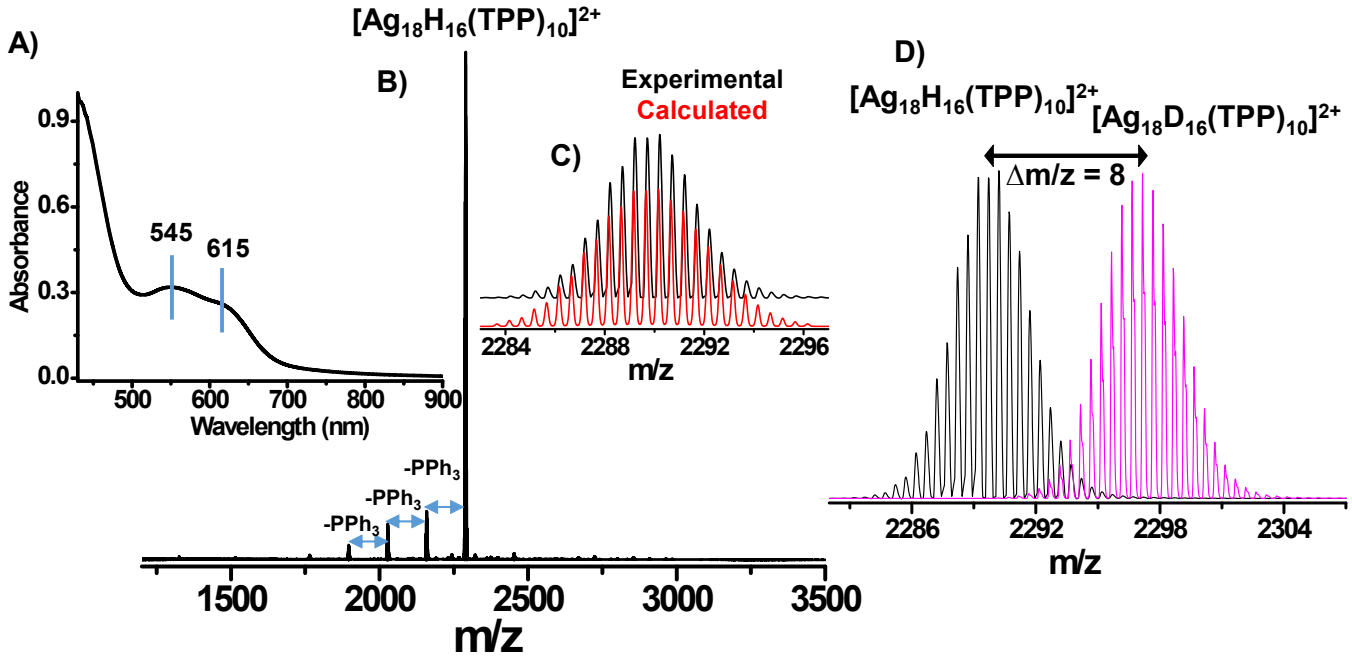

Fig. S1 A) UV-Vis absorption spectrum of $[Ag_{18}H_{16}(TPP)_{10}]^{2+}$ in MeOH showing two peaks at 545 nm and 615 nm. The characteristic absorption features are marked. B) ESI mass spectrum of $[Ag_{18}H_{16}(TPP)_{10}]^{2+}$ in positive ion mode (using the G2Si) showing a sharp molecular ion peak at m/z 2290 with 2+ charge state. Other small peaks arise due to PPh_3 losses from molecular ion peak. C) Expanded view of the m/z 2290 peak which shows the agreement between experimental and calculated isotopic patterns. D) ESI mass spectra of $[Ag_{18}H_{16}(TPP)_{10}]^{2+}$ and $[Ag_{18}D_{16}(TPP)_{10}]^{2+}$ clusters. The mass shift is $\Delta m/z = 8$ which is due to the exchange of 16 hydride ions with deuteride ions in 2+ charge state.

Supporting information 2

Experimental and calculated spectra of Ag_{17}^+, $[Ag_{17}(C\equiv CH)_2]^+$, $[Ag_{17}(C\equiv CH)_4]^+$ and $[Ag_{17}(C\equiv CH)_6]^+$:

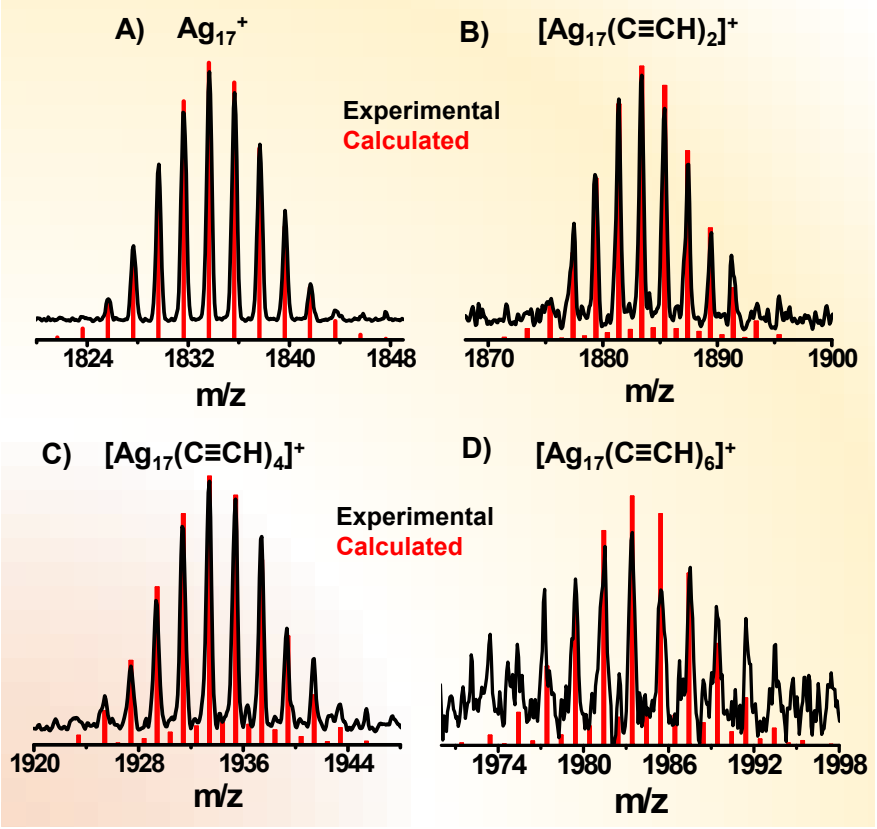

Fig. S2 The isotopic distribution of experimental (black) mass spectrum of A) Ag_{17}^+, B) $[Ag_{17}(C\equiv CH)_2]^+$, C) $[Ag_{17}(C\equiv CH)_4]^+$ and D) $[Ag_{17}(C\equiv CH)_6]^+$ matches well with their calculated (red) spectrum.

Supporting information 3

Full range ESI mass spectra during the reaction between naked clusters and acetylene:

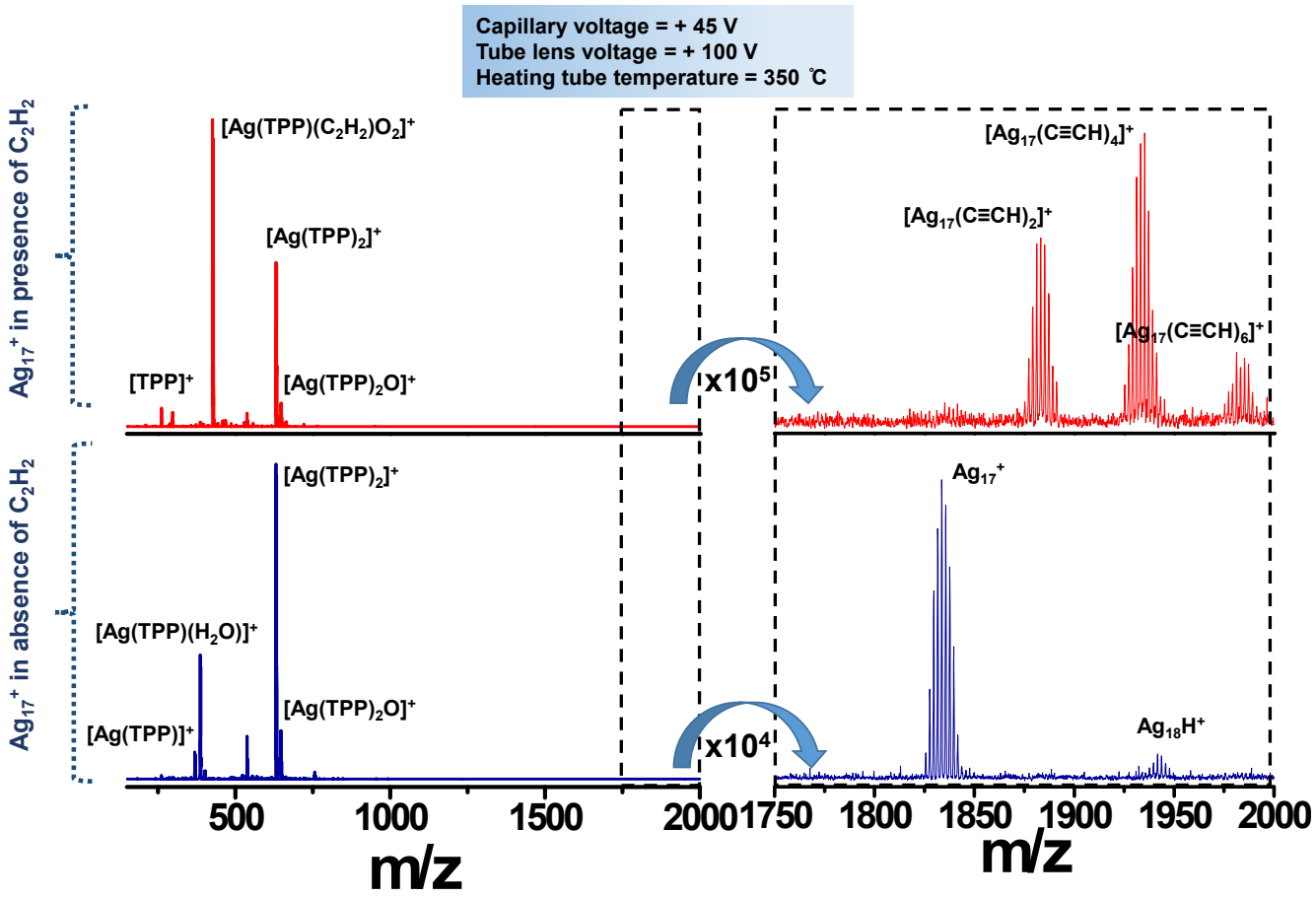

Fig. S3 Full range (150-2000 m/z) ESI mass spectra of naked clusters in absence and presence of acetylene gas. In absence of acetylene, there were naked cluster peaks of Ag_{17}^+ and $Ag_{18}H^+$ along with lower mass region peaks of $[Ag(TPP)]^+$, $[Ag(TPP)(H_2O)]^+$, $[Ag(TPP)_2]^+$ and $[Ag(TPP)_2O]^+$. In presence of acetylene, the lower mass peak $[Ag(TPP)(H_2O)]^+$ converted to $[Ag(TPP)(C_2H_2)O_2]^+$, where acetylene (C_2H_2) addition was observed. Whereas, for higher mass region, Ag_{17}^+ resulted only acetylide ($-C_2H$) addition peaks.

Supporting information 4A

Total CID pattern of $[Ag_{17}(C{\equiv}CH)_2]^+$:

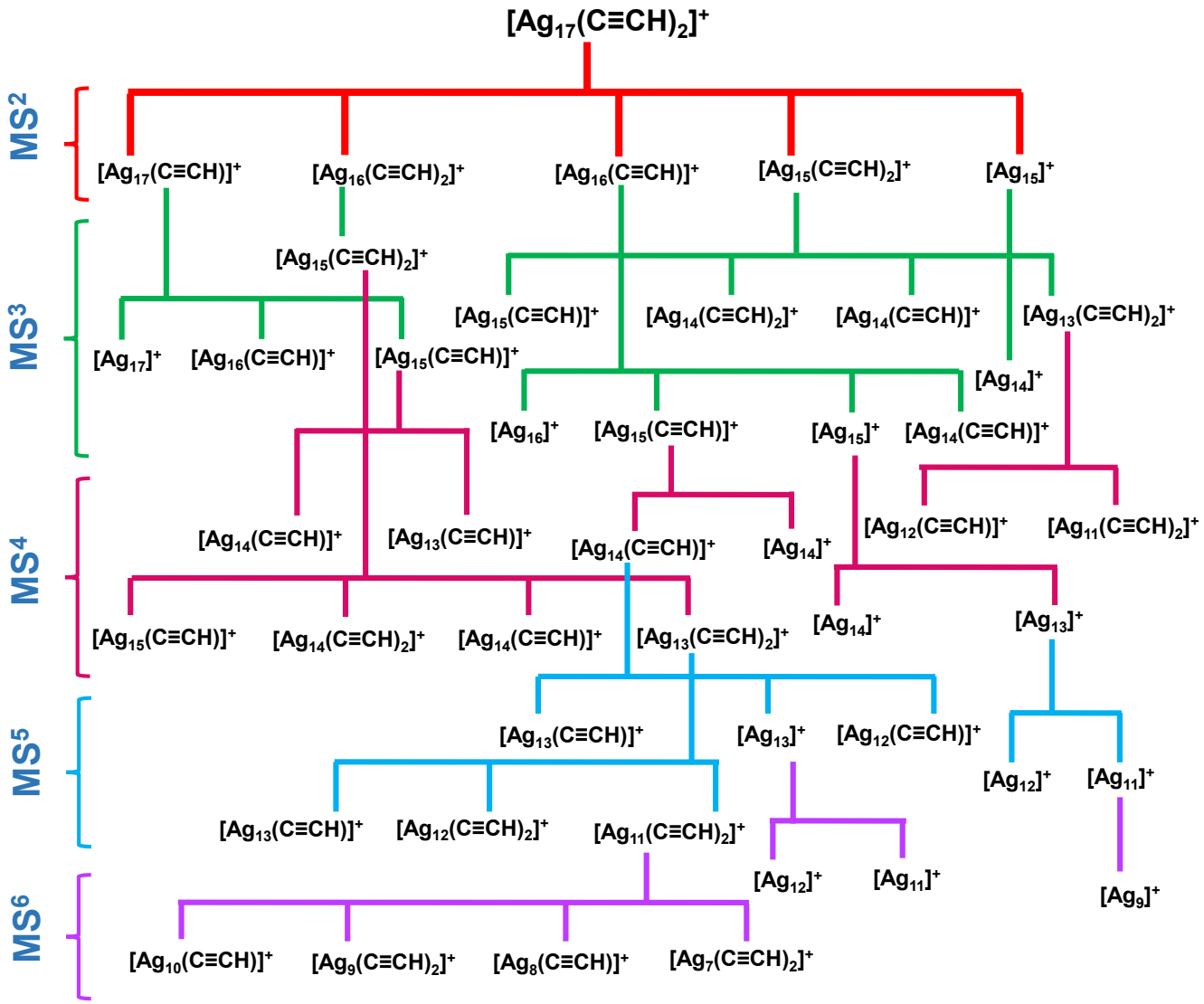

Fig. S4A Flow chart of the breaking pattern and fragments of the adduct $[Ag_{17}(C{\equiv}CH)_2]^+$, which were resulted by MS^2 to MS^6 experiments.

Supporting information 4B

Total CID pattern of $[Ag_{17}(C{\equiv}CH)_2]^+$:

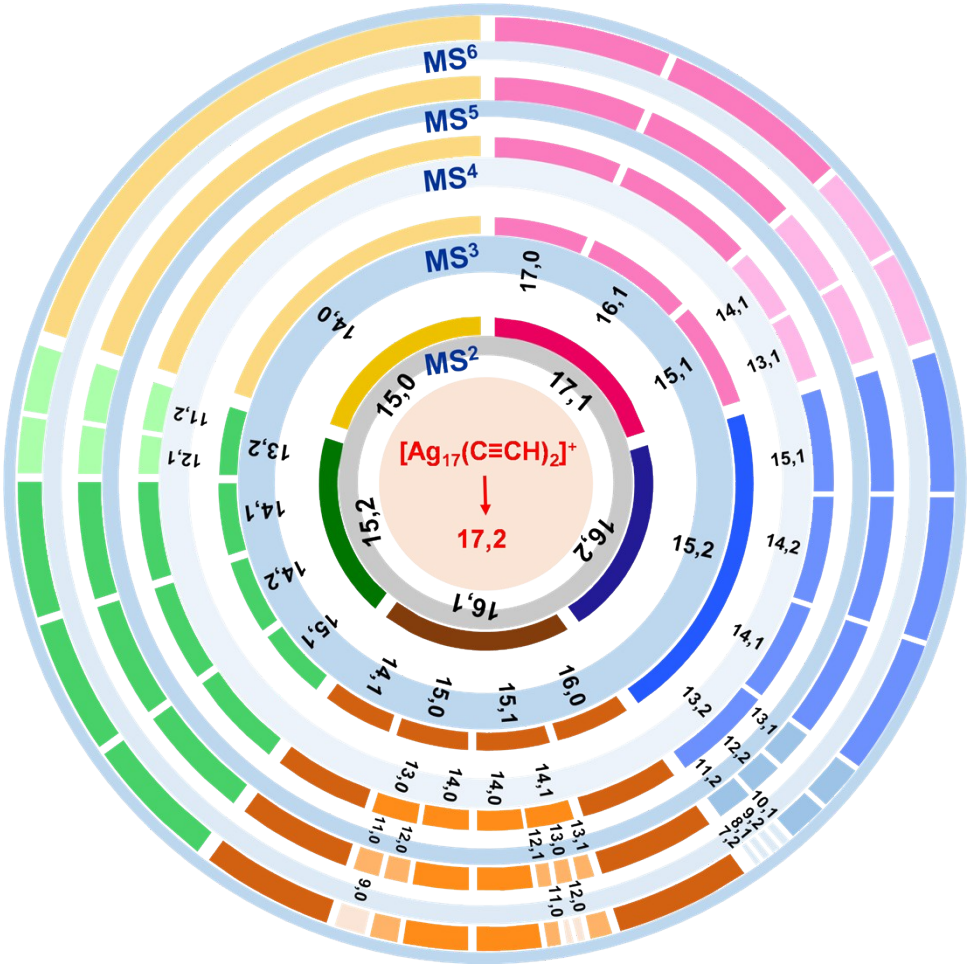

Fig. S4B The total CID fragments of $Ag_{17}(C{\equiv}CH)_2]^+$ or (17,2), resulting from MS^2 to MS^6 experiments are presented with five individual concentric rings. The first number represents the atomicity of the silver core and the second number represents the number of acetylide ($-C_2H$) ligands attached to it. The first level of fragmentation or MS^2 is shown in inner most ring with five different fragments. Then the next level of fragmentation continues with lighter shade of the same colour, ending at MS^6 level.

Supporting information 5

CID mass spectra of $[Ag_{17}(C{\equiv}CH)_2]^+$ through $[Ag_{17}(C{\equiv}CH)_1]^+$ pathway:

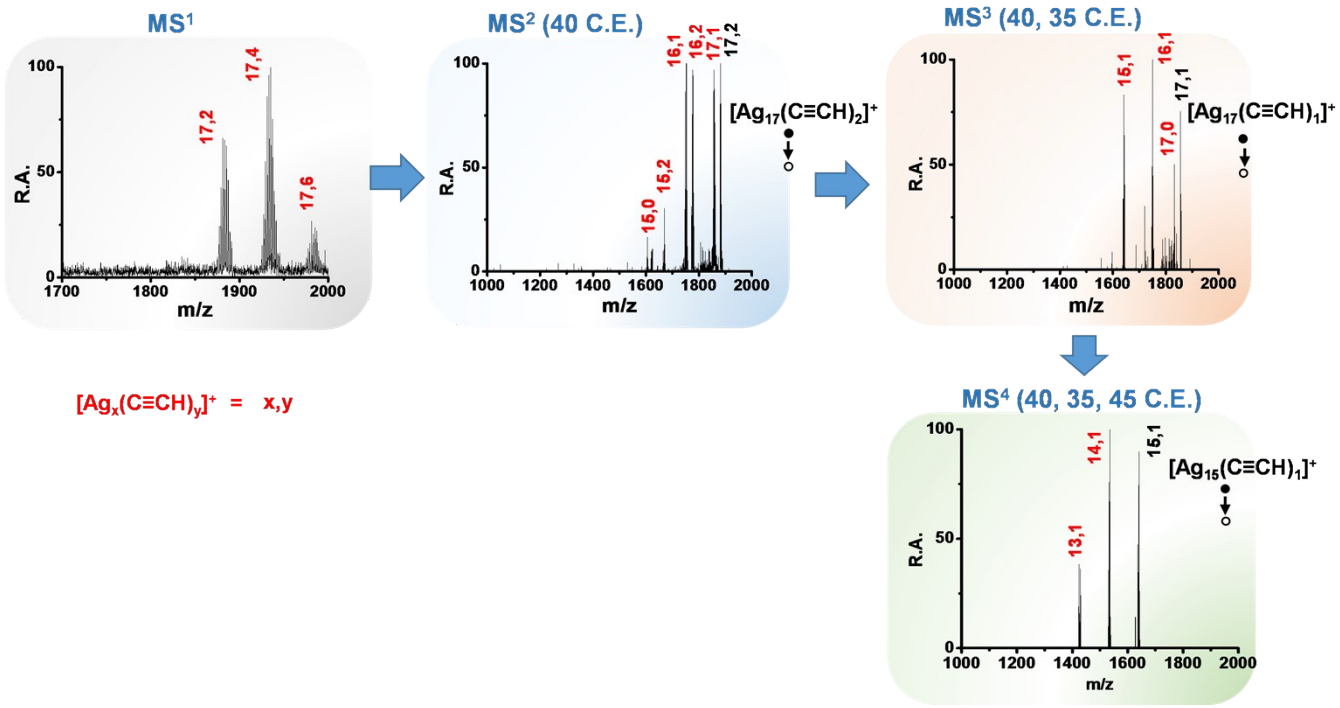

Fig. S5 MS^1 to MS^4 mass spectra of $[Ag_{17}(C{\equiv}CH)_2]^+$ or (17,2) through the (17,1) and (15,1) fragmentation pathway. The collision energy required to get the particular CID mass spectrum are written at the top of every mass spectrum. RA refers to relative abundance.

Supporting information 6

CID mass spectra of $[Ag_{17}(C{\equiv}CH)_2]^+$ through $[Ag_{16}(C{\equiv}CH)_2]^+$ pathway:

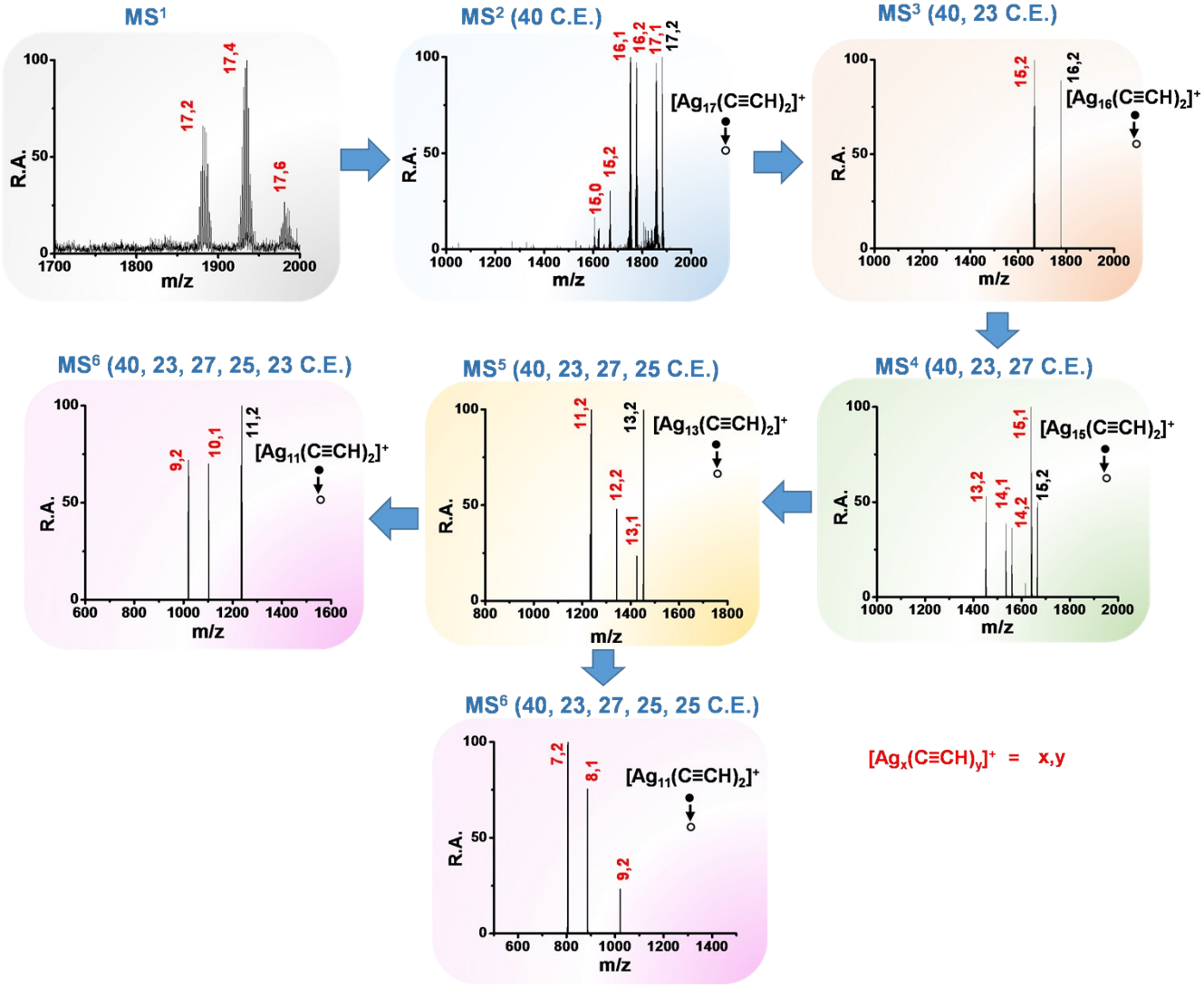

Fig. S6 MS^1 to MS^6 mass spectra of $[Ag_{17}(C{\equiv}CH)_2]^+$ or (17,2) through the (16,2), (15,2), (13,2) and (11,2) fragmentation pathway. The collision energy required to get the particular CID mass spectrum are written at the top of every mass spectrum. At the last step of MS^6, collision energy was changed from 23 to 25 to get different fragments, shown in two different MS^6 mass spectrum. RA refers to relative abundance.

Supporting information 7

CID mass spectra of $[Ag_{17}(C{\equiv}CH)_2]^+$ through $[Ag_{16}(C{\equiv}CH)_1]^+$ and followed by $[Ag_{15}(C{\equiv}CH)_1]^+$ pathway:

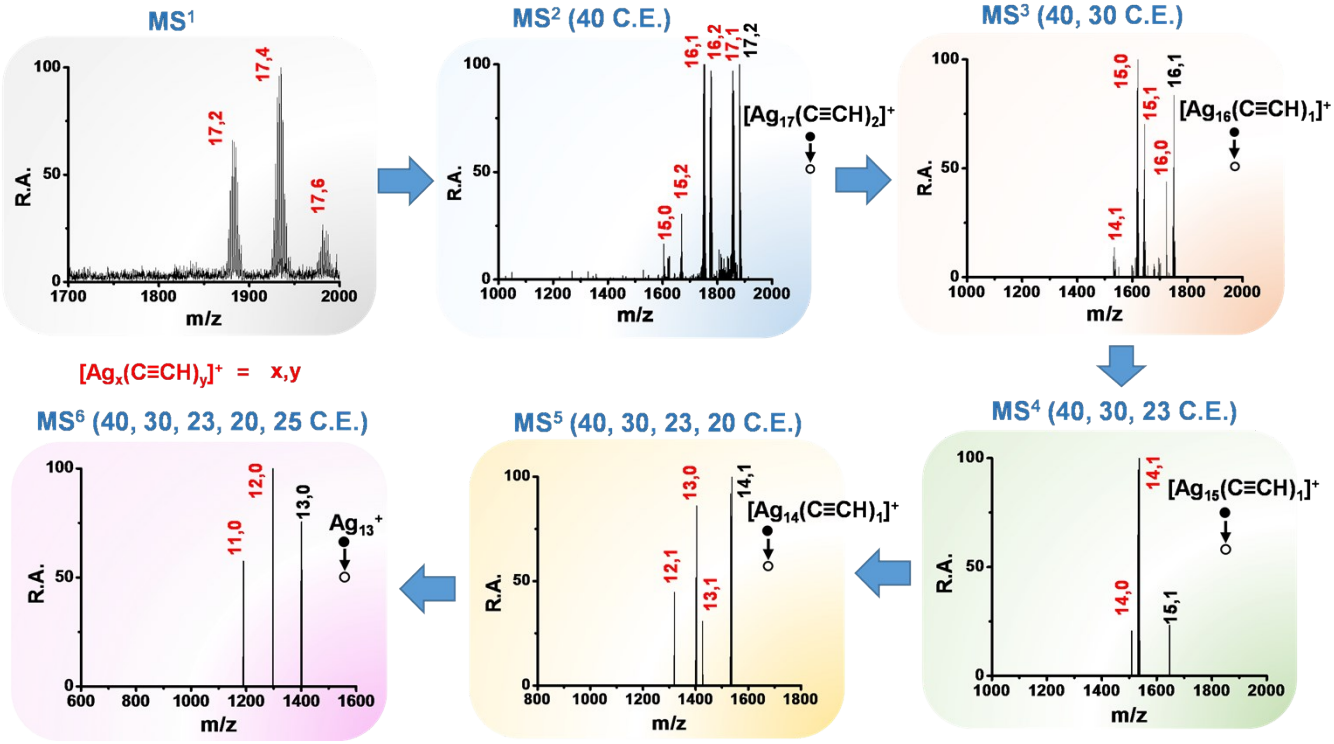

Fig. S7 MS^1 to MS^6 mass spectra of $[Ag_{17}(C{\equiv}CH)_2]^+$ or (17,2) through the (16,1), (15,1), (14,1) and (13,0) fragmentation pathway. The collision energy required to get the particular CID mass spectrum are written at the top of every mass spectrum. RA refers to relative abundance.

Supporting information 8

CID mass spectra of $[Ag_{17}(C{\equiv}CH)_2]^+$ through $[Ag_{16}(C{\equiv}CH)_1]^+$ and followed by $[Ag_{15}]^+$ pathway:

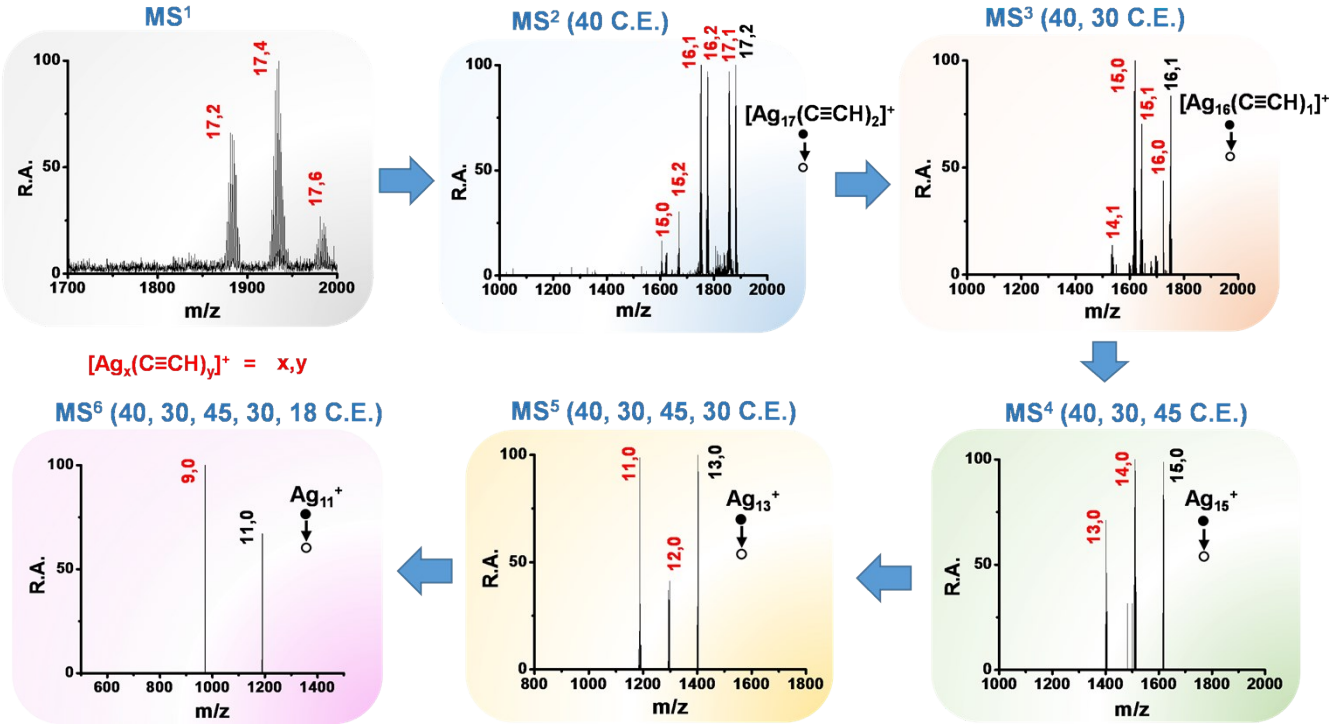

Fig. S8 MS^1 to MS^6 mass spectra of $[Ag_{17}(C{\equiv}CH)_2]^+$ or (17,2) through the (16,1), (15,0), (13,0) and (11,0) fragmentation pathway. The collision energy required to get the particular CID mass spectrum are written at the top of every mass spectrum. RA refers to relative abundance.

Supporting information 9

CID mass spectra of $[Ag_{17}(C\equiv CH)_2]^+$ through $[Ag_{15}(C\equiv CH)_2]^+$ pathway:

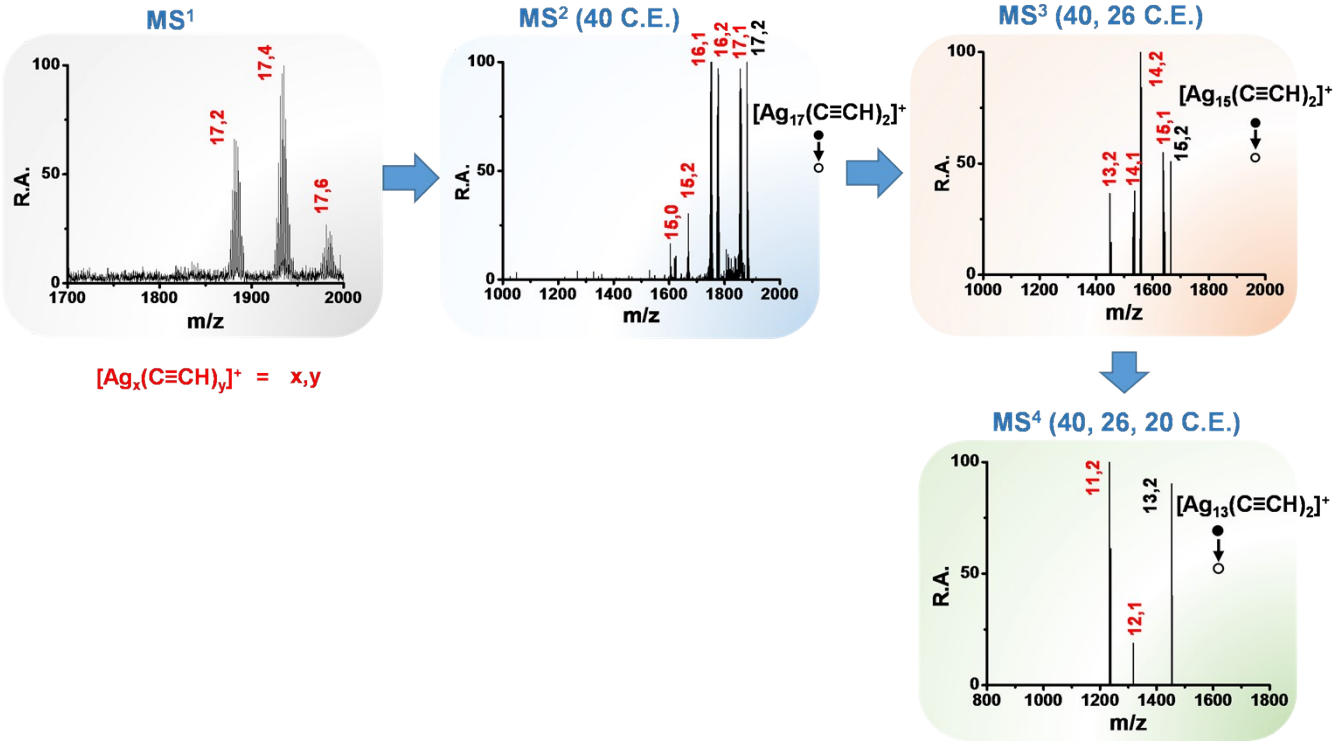

Fig. S9 MS^1 to MS^4 mass spectra of $[Ag_{17}(C\equiv CH)_2]^+$ or (17,2) through the (15,2) and (13,2) fragmentation pathway. The collision energy required to get the particular CID mass spectrum are written at the top of every mass spectrum. RA refers to relative abundance.

Supporting information 10

Total CID pattern of $[Ag_{17}(C{\equiv}CH)_4]^+$:

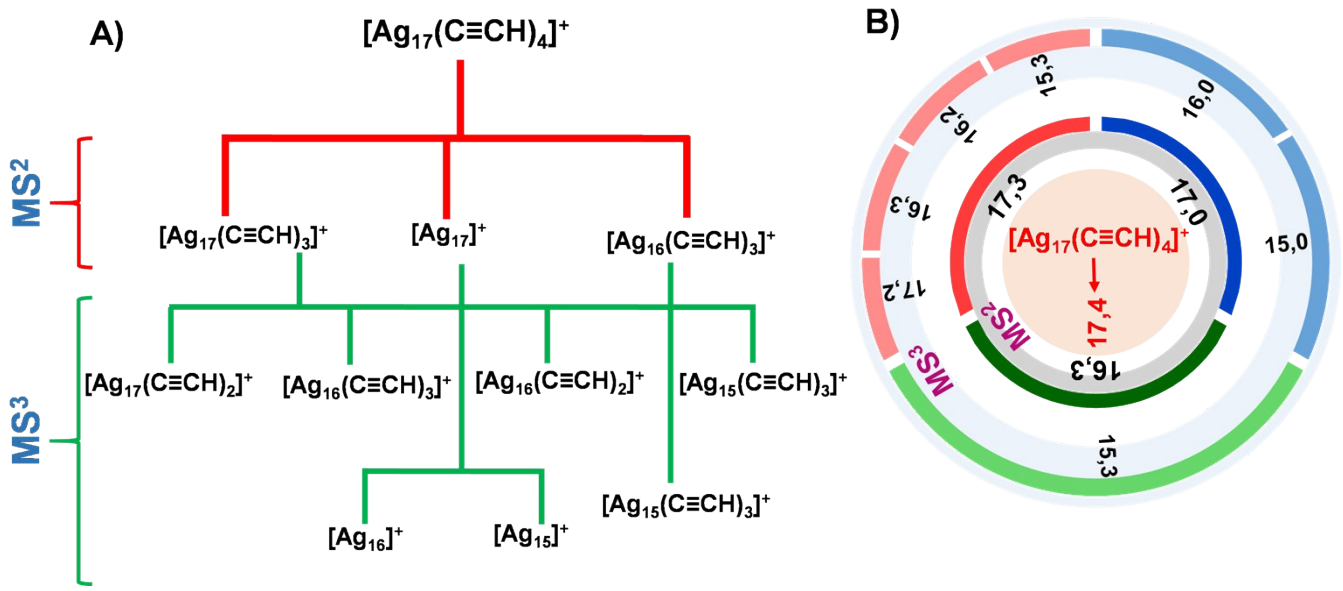

Fig. S10 A) Flow chart of the breaking pattern and fragments of the adduct $[Ag_{17}(C{\equiv}CH)_4]^+$, resulted from MS^2 and MS^3 experiments. B) The total CID fragments of $[Ag_{17}(C{\equiv}CH)_4]^+$ or (17,4) resulted from MS^2 and MS^3 experiments are presented with two individual concentric rings.

Supporting information 11

CID mass spectra of $[Ag_{17}(C{\equiv}CH)_4]^+$ up to MS^3:

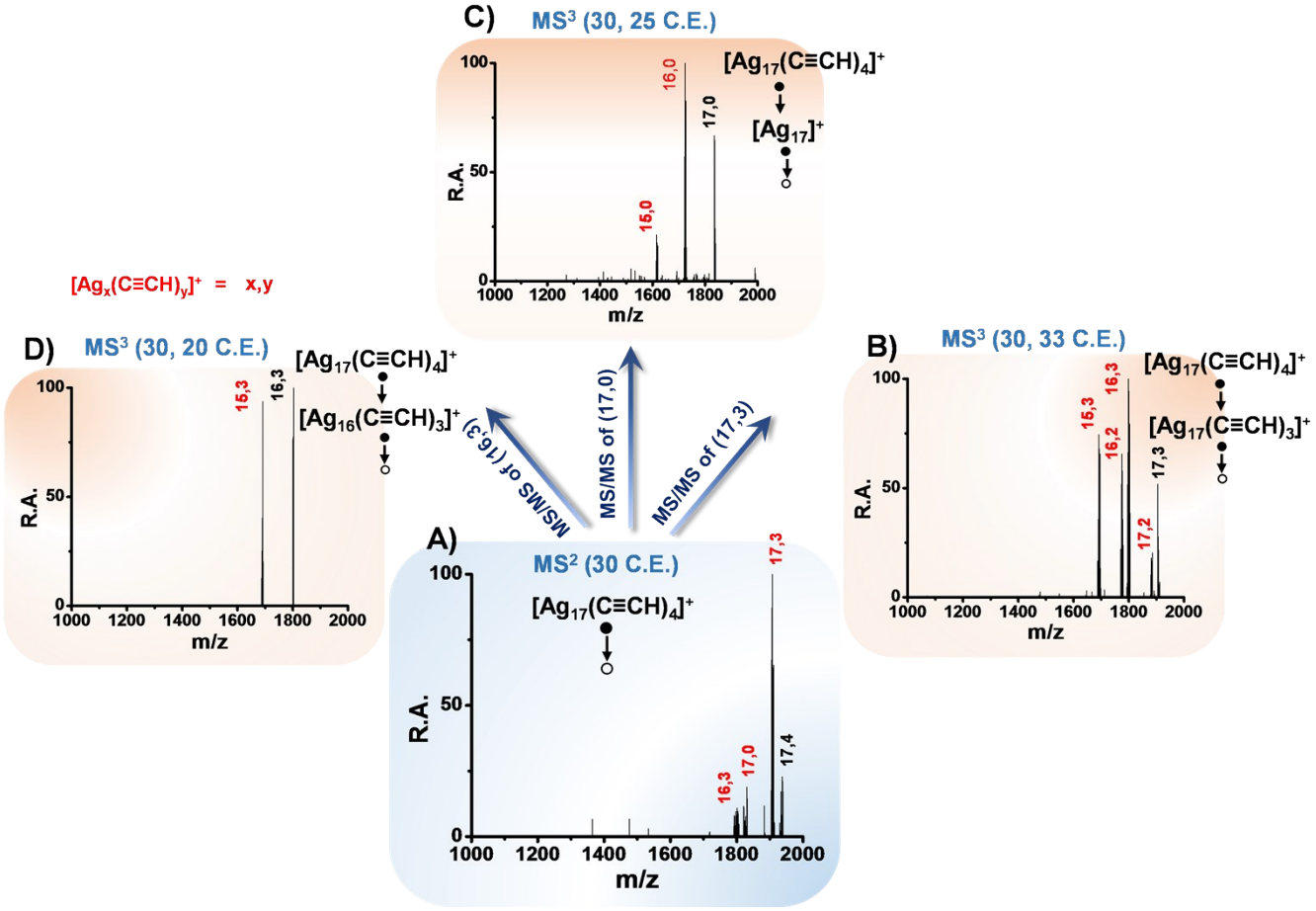

Fig. S11 A) MS^2 mass spectrum of $[Ag_{17}(C{\equiv}CH)_4]^+$ or (17,4), resulting three fragments of (17,3), (17,0) and (16,3). MS^3 mass spectrum of (17,3), (17,0) and (16,3) are also shown in B), C) and D), respectively. The collision energy required to get the particular CID mass spectrum are written at the top of every mass spectrum. RA refers to relative abundance.

Supporting information 12

Total CID pattern of $[Ag_{17}(C{\equiv}CH)_6]^+$:

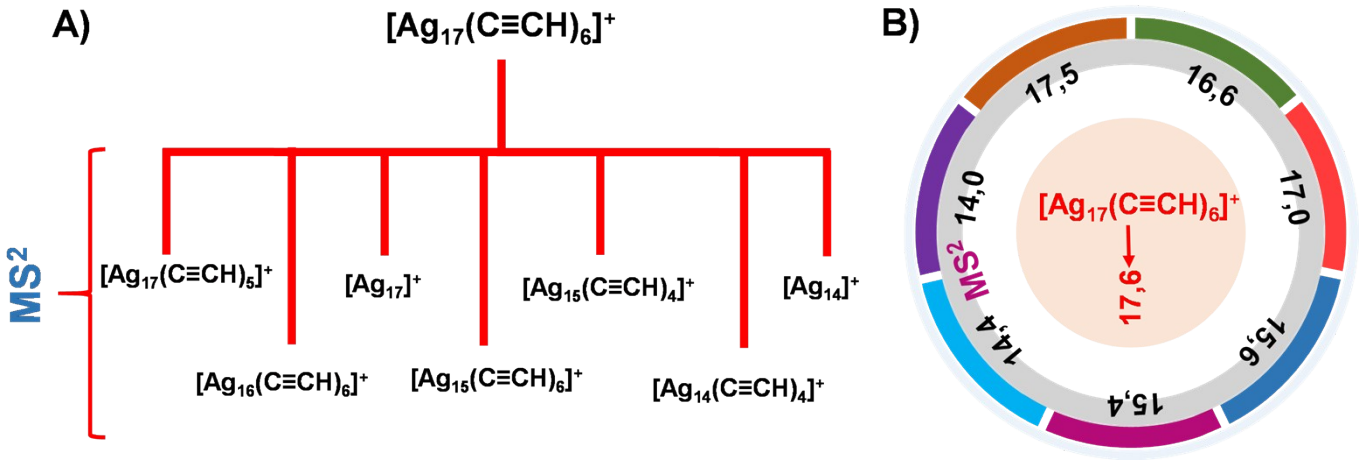

Fig. S12 A) Flow chart of the breaking pattern and fragments of the adduct $[Ag_{17}(C{\equiv}CH)_6]^+$, resulted from MS^2 experiment. B) The total CID fragments of $Ag_{17}(C{\equiv}CH)_6]^+$ or (17,6) resulting from MS^2 experiment is presented with one ring.

Supporting information 13

CID mass spectrum of $[Ag_{17}(C{\equiv}CH)_6]^+$ for MS^2:

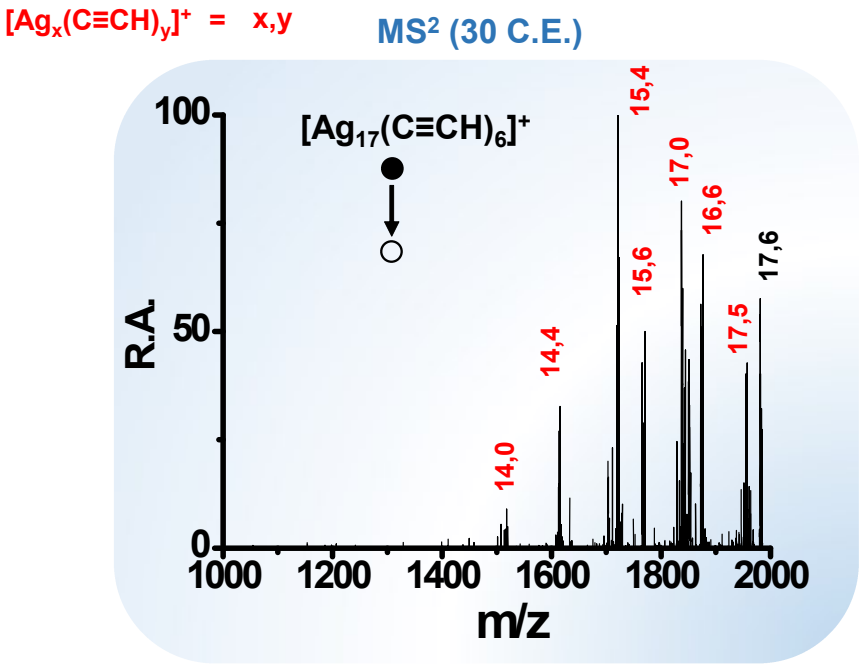

Fig. S13 MS^2 mass spectrum of $[Ag_{17}(C{\equiv}CH)_6]^+$ or (17,6), resulting seven fragments of (17,5), (16,6), (17,0), (15,6), (15,4), (14,4) and (14,0). The collision energy required to get the particular CID mass spectrum is written at the top of the spectrum. RA refers to relative abundance.

Table S14

Comparison of experimental and calculated masses measured with the LTQ:

In the isotopic cluster, the most abundant peak is used to define the m/z value.

Experimental m/z	Calculated m/z	Assignment $[Ag_m(PPh_3)_nH_o(H_2O)_pO_q(C_2H_2)_r(C_2H)_s]^{z+}$							
		Ag (m)	PPh_3 (n)	H (o)	H_2O (p)	O (q)	C_2H_2 (r)	C_2H (s)	Charge (z)
262.15	262.09		1						1
368.99	369.00	1	1						1
386.67	387.01	1	1		1				1
427.03	427.00	1	1			2	1		1
631.20	631.09	1	2						1
647.12	647.08	1	2			1			1
1833.12	1833.38	17							1
1883.30	1883.40	17						2	1
1933.33	1933.41	17						4	1
1983.33	1983.43	17						6	1
1943.41	1943.30	18		1					

Supporting information 15

Most stable calculated structures of reactant and products:

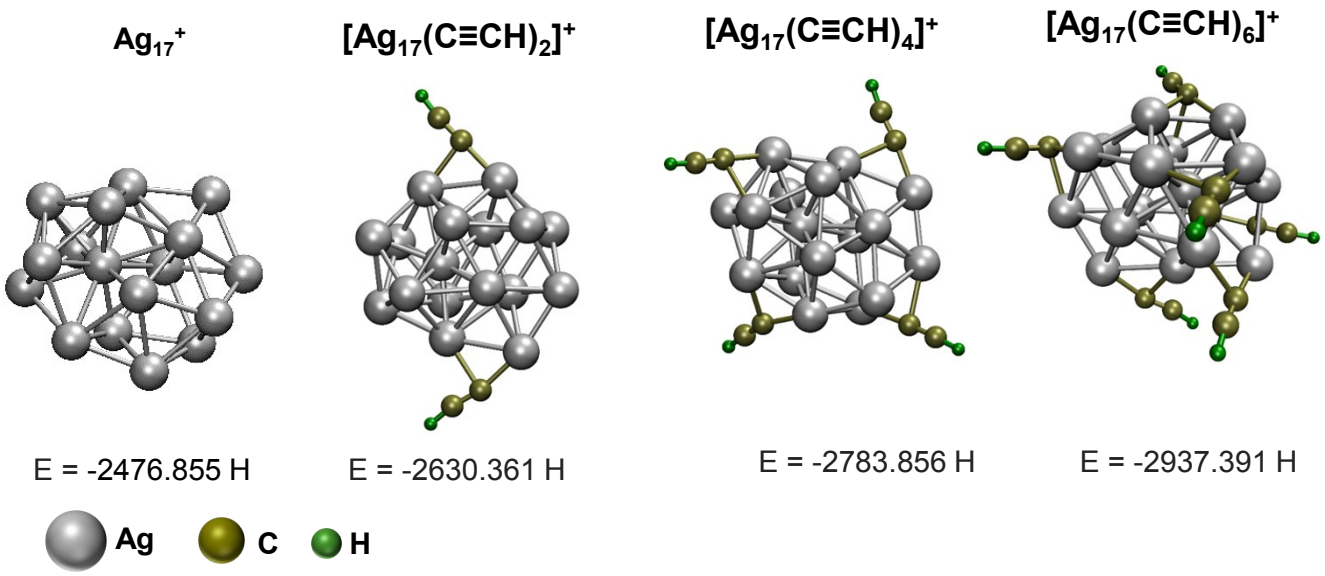

Fig. S15 Calculated most stable structures of Ag_{17}^+, $[Ag_{17}(C\equiv CH)_2]^+$, $[Ag_{17}(C\equiv CH)_4]^+$ and $[Ag_{17}(C\equiv CH)_6]^+$ with their calculated energy values. All the energy values are in Hartree.

Supporting information 16

HOMO-LUMO gap of reactant and products:

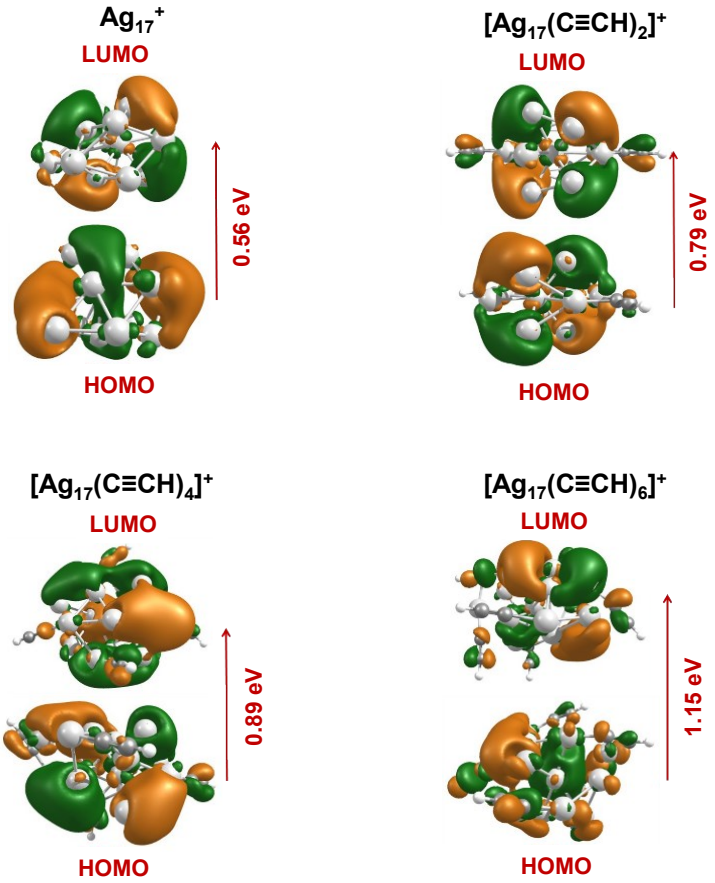

Fig. S16 HOMO-LUMO gap (ΔHL) of most stable structures of Ag_{17}^+, $[Ag_{17}(C\equiv CH)_2]^+$, $[Ag_{17}(C\equiv CH)_4]^+$ and $[Ag_{17}(C\equiv CH)_6]^+$. With increasing the number of attached $-C_2H$ unit to Ag_{17}^+, ΔHL value increases and for $[Ag_{17}(C\equiv CH)_6]^+$ it becomes highest, which makes it more resistive towards further reaction with acetylene.

Supporting information 17

Calculated structure of $[Ag_{17}(HC{\equiv}CH)]^+$ and $[Ag_{17}(HC{\equiv}CH)_2]^+$:

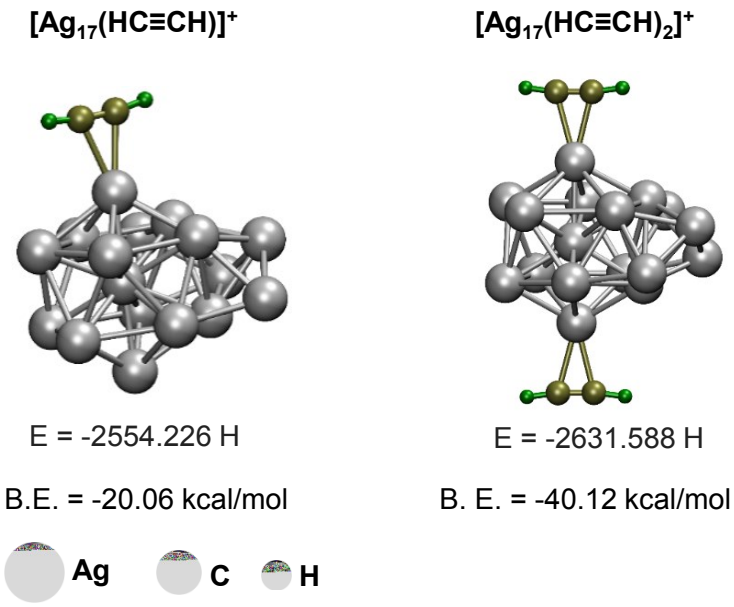

Fig. S17 Most stable calculated structures of $[Ag_{17}(HC{\equiv}CH)]^+$ and $[Ag_{17}(HC{\equiv}CH)_2]^+$ with their energy and binding energy values. The higher binding enrgy of $[Ag_{17}(HC{\equiv}CH)_2]^+$ refers to the higher stability compared to $[Ag_{17}(HC{\equiv}CH)]^+$. Energy values are in Hartree.

Supporting information 18

Possibility of formation of $[Ag_{17}(C{\equiv}CH)_2]^+$ and $[Ag_{17}C_4H_2]^+$:

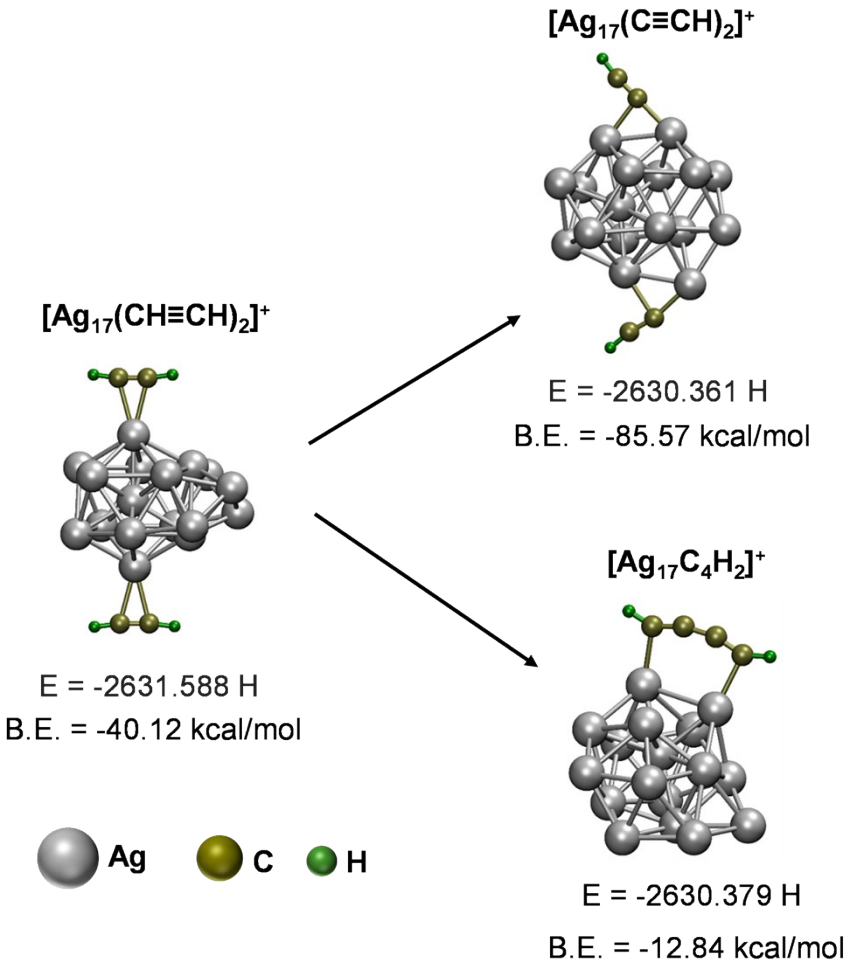

Fig. S18 After dehydrogenation of $[Ag_{17}(HC{\equiv}CH)_2]^+$, it can lead to the formation of either $[Ag_{17}(C{\equiv}CH)_2]^+$ or $[Ag_{17}C_4H_2]^+$ which are of same energy. But as $[Ag_{17}(C{\equiv}CH)_2]^+$ is having higher binding energy compared to $[Ag_{17}C_4H_2]^+$, the chance of formation of later becomes minimal.

Supporting information 19

Formation of $[Ag_{17}(C{\equiv}CH)_4]^+$ and hydrogen molecule:

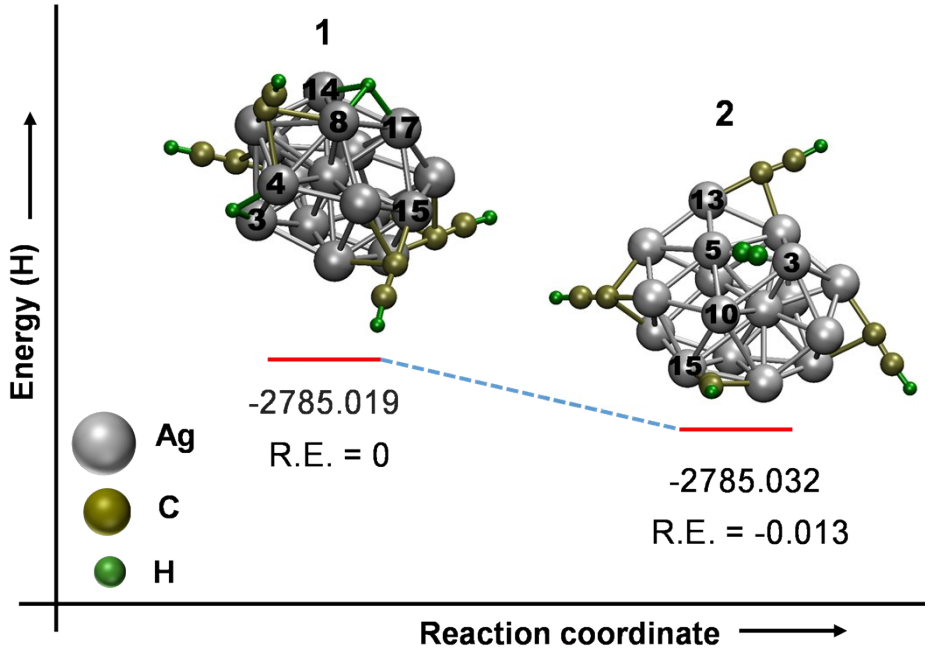

Fig. S19 Energy profile during the formation of $[Ag_{17}(C{\equiv}CH)_4]^+$ and hydrogen molecule (2) starting from the intermediate (1) of higher energy. The energy difference between the product and intermediate is 0.013 H. The exact energy and relative energy values are in Hartree.

Supporting information 20

Formation of $[Ag_{17}(C{\equiv}CH)_6]^+$ and hydrogen molecule:

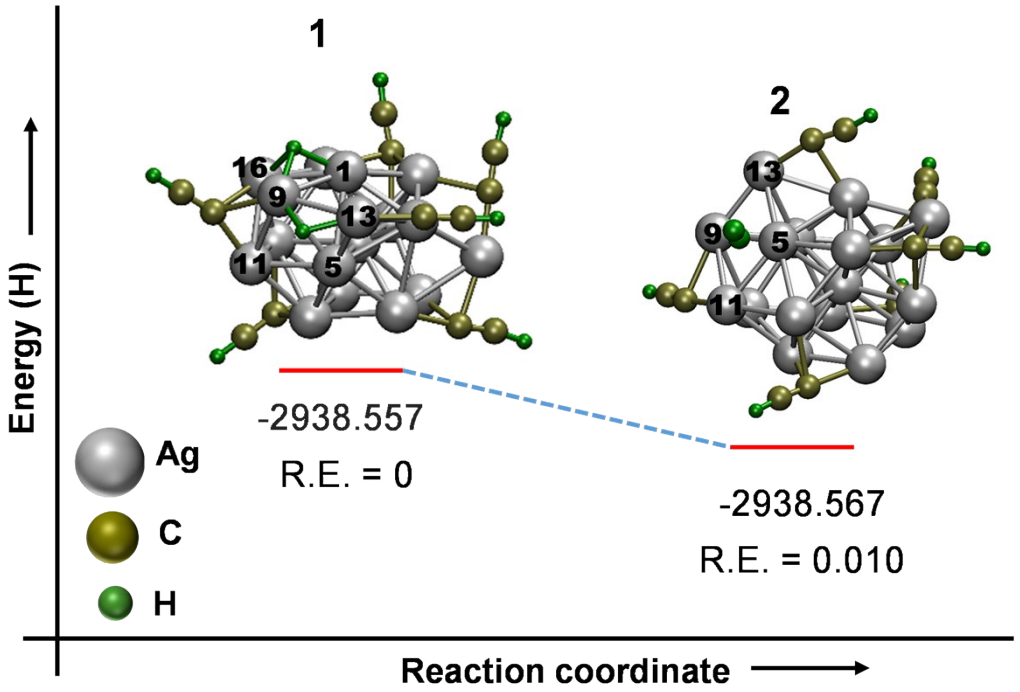

Fig. S20 Energy profile during the formation of $[Ag_{17}(C{\equiv}CH)_6]^+$ and hydrogen molecule (2) starting from the intermediate (1) of higher energy. The energy difference between the product and intermediate is 0.010 H. The exact energy and relative energy values are in Hartree.

Supporting information 21

Energy profile of overall reaction:

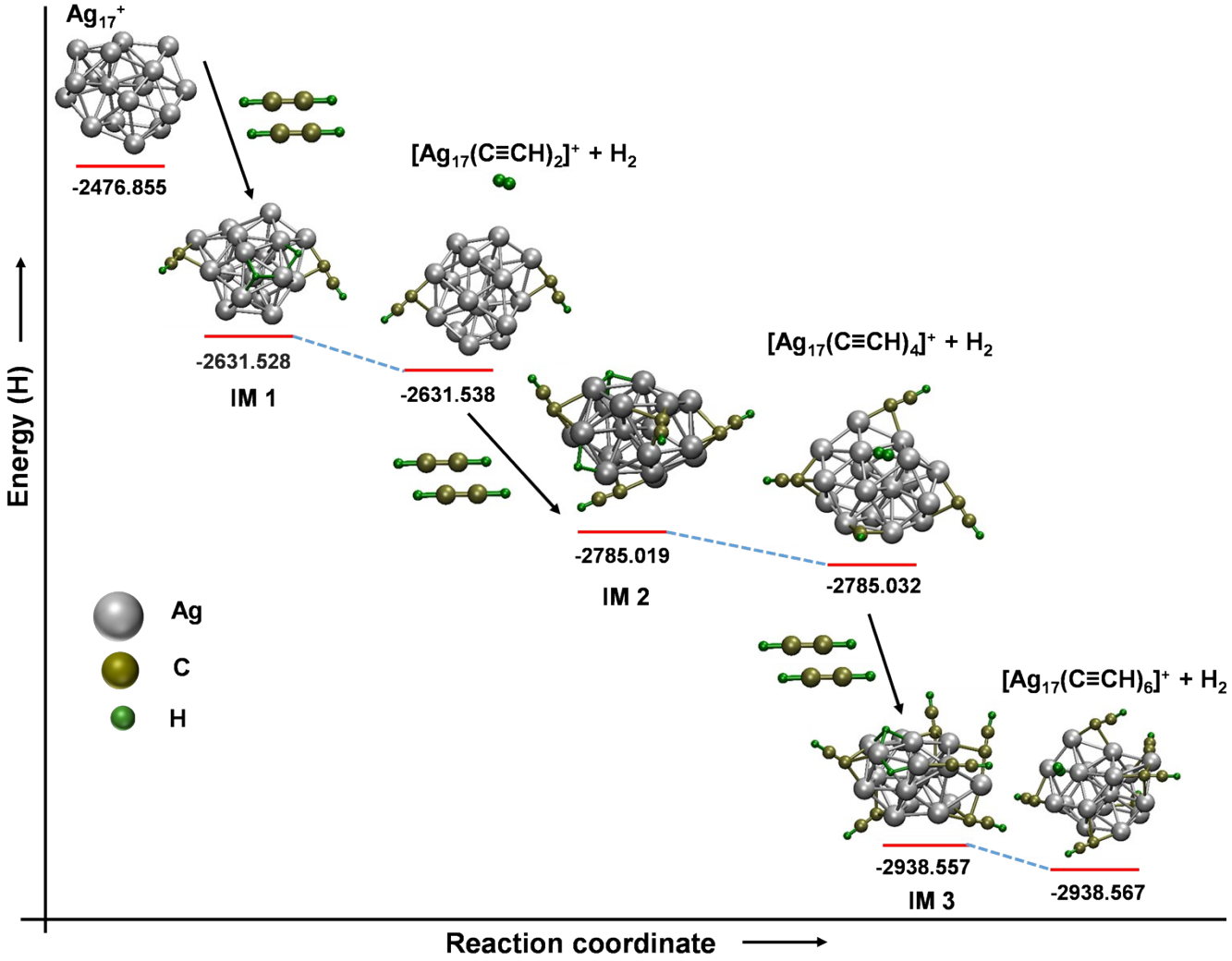

Fig. S21 Energy profile during the overall reaction between Ag_{17}^{+} and acetylene. The exact energy of the reactant Ag_{17}^{+}, intermediates (IM) and products are in Hartree. This profile shows that with increasing the number of attached $–C_2H$ unit to Ag_{17}^{+}, the energy got decreased starting from the free Ag_{17}^{+} to $[Ag_{17}(C{\equiv}CH)_6]^{+}$ consecutively.

Supporting information 22

Possibility of formation of $[Ag_{17}(C{\equiv}CH)]^+$:

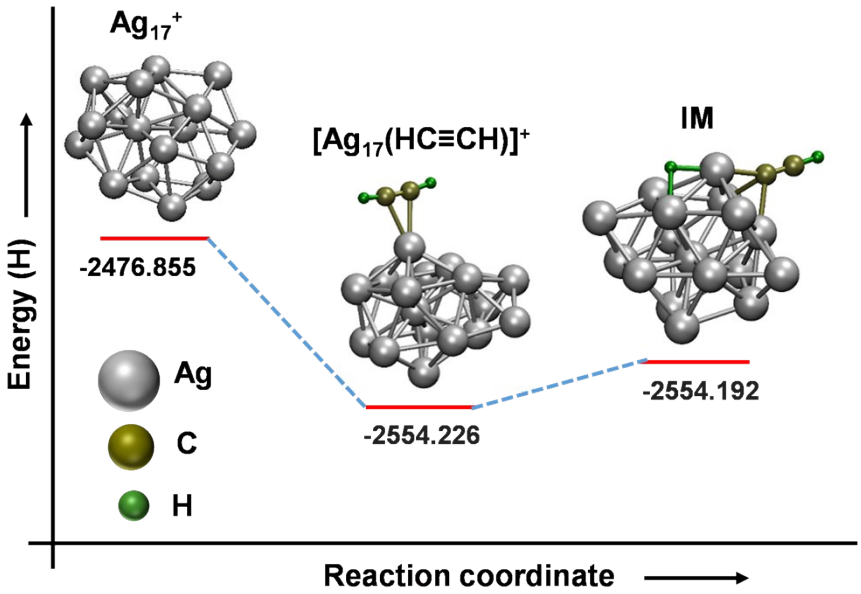

Fig. S22 Energy profile during the formation of $[Ag_{17}(HC{\equiv}CH)]^+$ from Ag_{17}^+ and and its dehydrogenation, giving the higher energy intermediate (IM). The intermediate does not end up to any stable lower energy product in the case of odd (one) number of attached acetylene molecule. The energy values are in Hartree.

Table S23

Calculated binding energies:

Cluster + C_2H	**Binding Energy (kcal/mol)**
$[Ag_{17}(C{\equiv}CH)]^+$	-79.90
$[Ag_{17}(C{\equiv}CH)_2]^+$	-85.57
$[Ag_{17}(C{\equiv}CH)_4]^+$	-83.04
$[Ag_{17}(C{\equiv}CH)_6]^+$	-86.43

Supporting information 24

Calculated structures of precursor and product ions during CID:

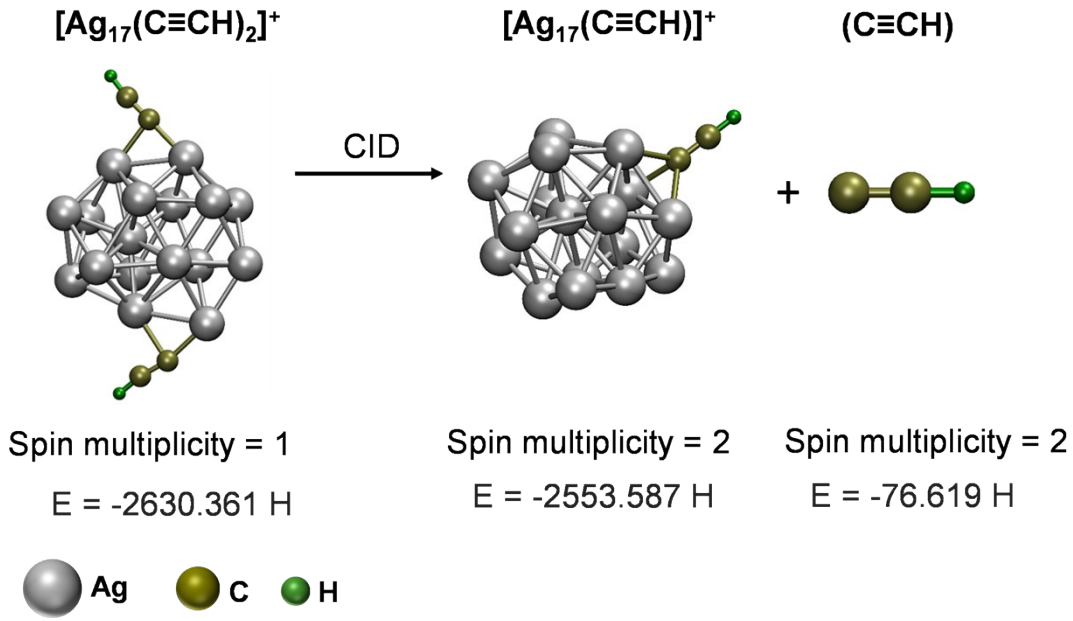

Fig. S24 Structures of precursor and product ions during the CID event. Calculated structures of $[Ag_{17}(C{\equiv}CH)_2]^+$, $[Ag_{17}(C{\equiv}CH)]^+$ and [C≡CH)] with their spin multiplicity and calculated energy values. All the energy values are in Hartree.

Supporting information 25

Electronic structure of $[Ag_{17}(C{\equiv}CH)_2]^+$:

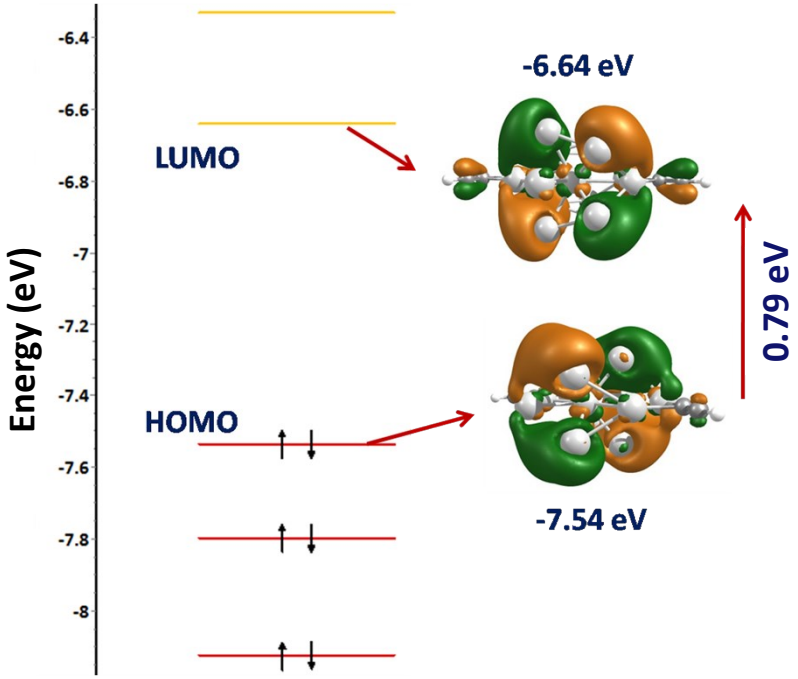

Fig. S25 The electronic structure (closed-shell) and HOMO-LUMO gap of $[Ag_{17}(C{\equiv}CH)_2]^+$. The electronic shell structure is | $1S^2$ | $1P^6$ | $1D^6$ |.

Supporting information 26

Electronic structure of $[Ag_{17}(C{\equiv}CH)]^+$:

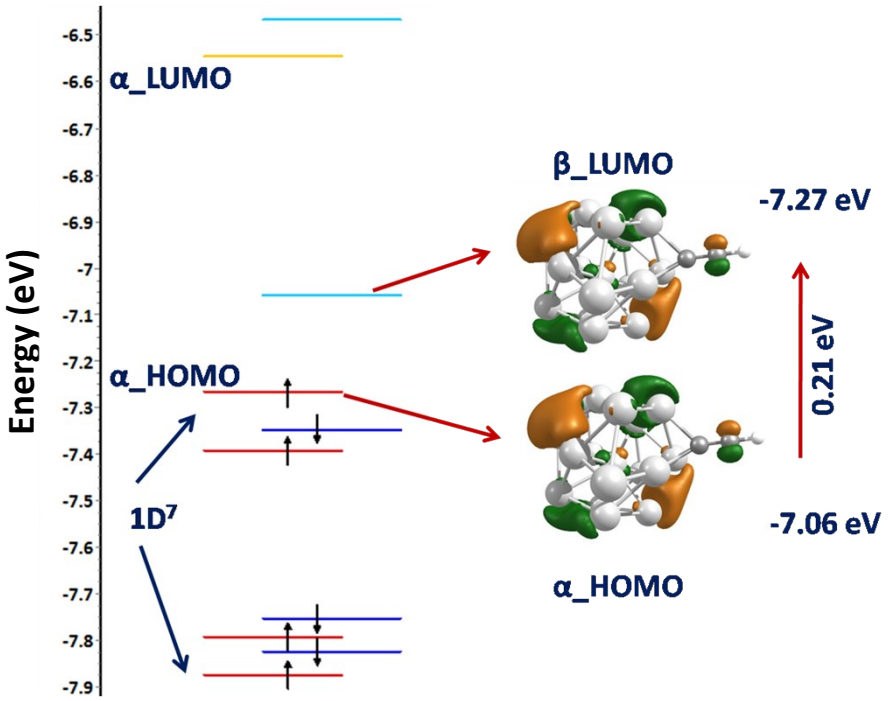

Fig. S26 The electronic structure (open-shell) and HOMO-LUMO gap of $[Ag_{17}(C{\equiv}CH)]^+$. The electronic shell structure is | $1S^2$ | $1P^6$ | $1D^7$ |.

Supporting information 27

Electronic structure of [C≡CH]:

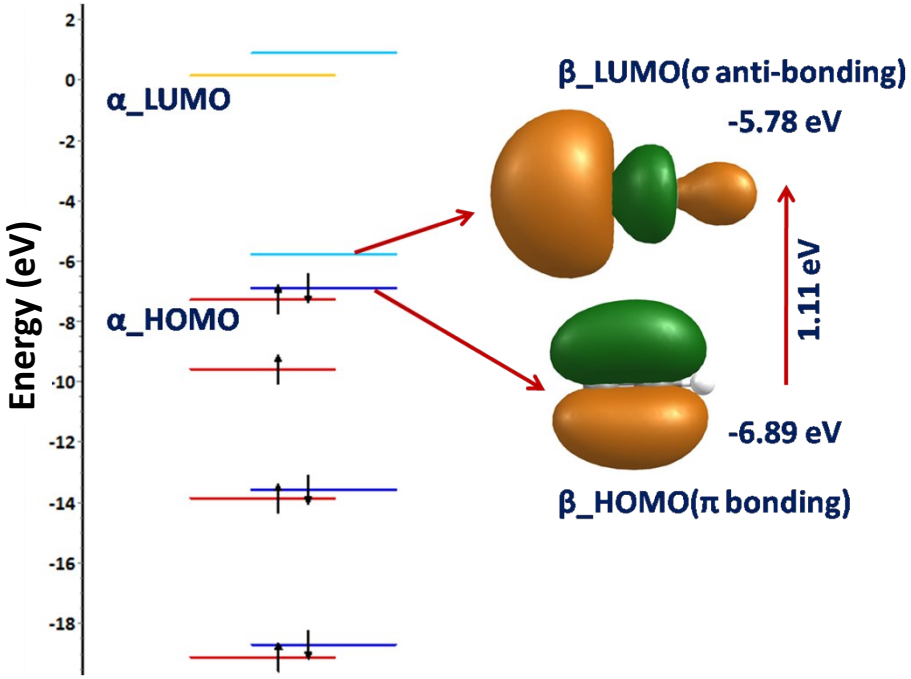

Fig. S27 The electronic structure (open-shell) and HOMO-LUMO gap of [C≡CH].